Compressing PEG Brushes

Tanja Drobek,* Nicholas D. Spencer, and Manfred Heuberger

Laboratory for Surface Science and Technology, Department of Materials, ETH Zürich, Wolfgang-Pauli-Strasse 10, CH-8093 Zürich, Switzerland

Received February 28, 2005; Revised Manuscript Received April 19, 2005

ABSTRACT: Poly(ethylene glycol) (PEG) surface grafts are used as surface coatings that impart resistance to nonspecific protein adsorption. In this work, brushes of poly(ethylene glycol), grafted to a cationic polylysine backbone and adsorbed onto mica, were investigated with the surface forces apparatus, providing direct measurements of forces and refractive index via thin-film interferometry. Surface force isotherms were measured for different molecular architectures. The temperature dependence of the film thickness was also studied. The observed interaction force is predominantly repulsive and nearly elastic and can be described by polymer−brush scaling theory. Comparisons between polymer−polymer and polymer−hard-wall compression isotherms show a significant interpenetration of the two polymer films.

Introduction

Poly(ethylene glycol) (PEG) is a water-soluble polymer with the repeat unit (−CH_2−CH_2−O−). Its water solubility is known to be linked to its structural properties, and it is unique in the family of comparable polyethers since both poly(methylene glycol) (−C−O−) and higher glycols are insoluble in water.[1]

PEG chains grafted to the surface at a sufficiently high density form a brushlike layer because the lateral interactions between the hydrated chains cause them to extend. These brushes are of great technological importance: The steric repulsion can be exploited for the stabilization of colloid particles in suspensions,[2] and the brushlike films also form an effective barrier to the adsorption of macromolecules. The ability of PEG films to reduce the adsorption of proteins onto surfaces has opened a broad field of applications in biotechnology.[3] Surface-grafted PEG films are also of interest for tribological applications since they contain a layer of bound water, which drastically influences the lubrication properties.[4−6]

In a good solvent different film structures can occur for a surface-grafted polymer film, depending on the surface coverage.[7] At low coverages, the molecules behave like isolated chains. If the interaction between the polymer chains and the surface is negligible, as in the case of short PEG chains on mica in an aqueous environment, the polymer chains adopt a mushroom conformation. The extension of the polymer into solution is comparable in diameter to that of an isolated molecule in solution, described as R_g, the unperturbed radius of gyration. At higher surface coverages the polymer chains start to interact with each other. In the semidilute regime, the unperturbed chains overlap, and the excluded-volume effect forces them to extend into a brushlike configuration.[8] In the limit of high surface coverage, the polymer chains are completely stretched out. To balance the strong repulsive forces between the chains, the grafting of the chain onto the surface must be very stable. Therefore, such high surface coverages are challenging to achieve experimentally.[7,9]

The grafting strategy we have employed is based on chemically grafting the PEG chains onto a polyelectrolyte chain via an amide linkage. In the present study poly-L-lysine was used as a backbone. In Figure 1, the building blocks of the copolymer are shown. In aqueous solution the copolymer adsorbs via electrostatic interaction onto oppositely charged surfaces such as metal oxides or mica. This grafting strategy was originally developed for improving the biocompatibility of microcapsules.[10] The density of the adsorbed film is a result of the balance between the electrostatic attraction of the backbone and the steric repulsion of the PEG chains. It depends on the architecture of the copolymer as well as on the surface charge density of the substrate and the properties of the solvent.[11−13]

Here we report details of the interaction of two opposing PLL-*g*-PEG layers that are brought into contact with each other, a geometry which is relevant for tribological applications or the contact of polymer-stabilized colloidal particles. The effect of PEG chain length and temperature was studied. A comparison between the compression of a single brush by a hard wall with the compresion of two brushes is made to study the effect of interpenetration. The two architectures studied here consist of relatively short poly-L-lysine backbones grafted with PEG with 2 or 5 kDa. From aqueous solution they both adsorb with a sufficiently high density on the surface. In a "good solvent" such as water, these films are in a brushlike configuration in the semidilute regime.

Experimental Section

Polymer Film. The molecules used in this study were synthesized and characterized according to the standardized procedures previously described in great detail.[12,14,15] For this work two different molecular architectures were used: PLL(20)-g[2.9]-PEG(2), which is the optimum architecture for protein-resistant coatings on oxide surfaces,[12] and PLL(20)-g[3.5]-PEG(5), which has shown a remarkably good performance as a lubricious coating on aqueous environment.[6]

The notation adopted here, PLL(*a*)-g[*b*]-PEG(*c*), refers to the stoichiometry of the PLL-*g*-PEG molecule, indicating the average molecular weight *a* (given in kDa) of the poly(L-lysine) backbone as a hydrobromide salt used for the synthesis, the grafting ratio *b,* which is the average number of lysine units per side chain, and the average molecular weight of the PEG chains *c* (in kDa). The molecules used for this study contain a 94 Lys-mer. The side chains consist of PEG 44-mers (PEG(2)) and 114-mers (PEG(5)), both terminated with a methoxy

* Corresponding author: Tel +4116326449; Fax +4116331027; e-mail tanja.drobek@mat.ethz.ch.

10.1021/ma0504217 CCC: $30.25
Published on Web 05/19/2005

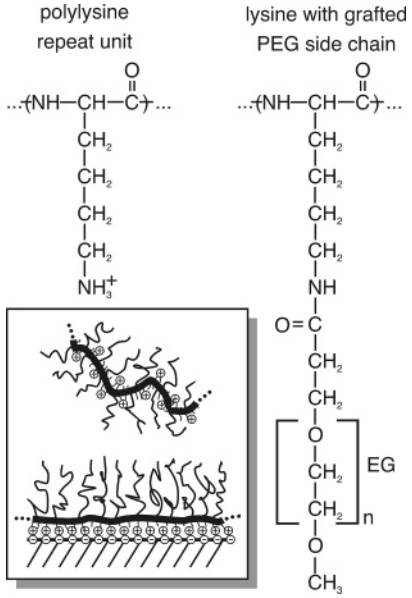

Figure 1. Repeat units of the PLL-*g*-PEG molecule. Each copolymer contains in average 94 lysine repeat units and about 27 (grafting ratio 3.5) or 32 (grafting ratio 2.9) grafted PEG chains. The PEG(2) side chains contain on average 45 CH_2-CH_2-O units, and the PEG(5) side chains consist of 114 units. Inset: on negatively charged surfaces, the polylysine backbone adsorbs on the substrate, and the PEG side chains form a brushlike structure.

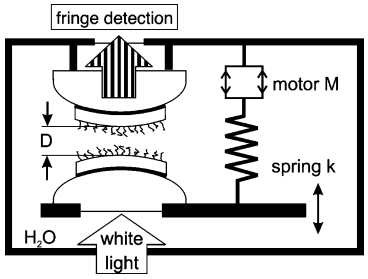

Figure 2. Schematic drawing of the SFA experimental setup. One surface is mounted on a spring, the base of which can be moved by a motor. The two mica surfaces are coated with a 40 nm thick layer of silver on the far side. The separation of the two mica surfaces can be readily measured in this thin-film interferometer.

group. Both batches of PEG used for the synthesis have a polydispersity of M_w/M_n below 1.1. The polydispersity of the poly(L-lysine) backbone is higher ($M_w/M_n = 1.3$). Because of the synthesis process, small variations of the grafting ratio are to be expected, although this is hard to verify experimentally since the polydispersity of the entire copolymer is dominated by variations in the backbone length.[15]

At pH 5.5, lysine units without grafted PEG chains all carry positive charges. The density of the adsorbed film is determined by the balance between the strong electrostatic interaction of the backbone with the negatively charged mica substrate and the steric repulsion of the PEG chains when they are forced to stretch to avoid overlapping. Since the adsorption process is random, a distribution of the grafting distances is expected.

Surface Forces Apparatus. The extended surface forces apparatus (eSFA) used for the experiments reported here is an enhanced and automated version of the SFA 3 (Surforce, Santa Barbara, CA).[16] In the SFA technique (Figure 2), the distance between two surfaces is measured with multiple-beam interferometry.[17] The interferometric distance determination was carried out with a fully automated spectrum aquisition and evaluation system, using a linear high-resolution CCD camera and applying a numerical fast spectral correlation (FSC) algorithm based on the optical multilayer matrix theory.[18] Our setup allows for a measuring rate of 1−2 data points per second with a precision of $\sigma_D = \pm 25$ pm for the distance and $\sigma_n = \pm 0.05$ for the refractive index determination.

Compression isotherms with typical approach and retract rates of 1 nm/s were measured in aqueous solution at controlled temperatures. In contact, the normalized surface force $F/R(D)$ was determined from

$$\frac{F(D)}{R} = \frac{k}{R}(D - M) = 2\pi E(D) \quad (1)$$

where the compliance of the force-measuring spring $k = 1002 \pm 23$ N/m and the effective radius $R = (R_x R_y)^{0.5}$, representing the local surface curvature, were used for normalizing the force. M is the calibrated motor position. On the basis of the Derjaguin approximation[19,20] $F/R \approx 2\pi E(D)$, the free energy per unit area $E(D)$ can be estimated.

The calculation of the free energy is subject to errors (e.g., motor nonlinearity, drift, geometry). A detailed error estimation has been published elsewhere.[21] Here, the accuracy of $F(D)/R$ is mainly limited by small motor nonlinearities to typically ±0.1 mN/m.

The eSFA is located inside a thermally insulated enclosure at a controlled temperature with a stability of ±20 mK/h in the box and ±2mK/h in the SFA body.[22] The temperature difference between the interferometer and the rest of the sealed SFA interior is about 400 mK due to heating of the water in the fluid cell by the light source.

Sample Preparation. For the preparation of the mica surfaces (optical quality ruby mica, Spruce Pine) a cutting procedure with scissors was used in order to avoid the formation of nanoparticles reported to occur for the standard preparation procedure.[23−25] The mica sheets were covered on one side with a 40 nm silver film. They were glued onto cylindrical glass lenses with a spin-coated film of pure epoxy resin (EPON 1004, Shell Chemicals) heated to 140 °C and inserted into the SFA within 5 min after gluing. The SFA was purged with dry nitrogen for at least 1 h. The optical thickness of the mica surfaces was determined in a dry nitrogen atmosphere in an unloaded adhesive contact at 25.00 °C. This thickness was used as a reference for the following measurements. The correction for the thermal expansion of the interferometer was 1.2×10^{-5} μm^{-1} $°C^{-1}$.

After separating the surfaces, the SFA was filled with ultrapure water (puris. p.a., 0.2 μm membrane filtered, Fluka, Milwaukee, WI, used as received). A stainless steel container was used for a slow transfer of the aqueous solutions into the sealed eSFA through a closed circuit using a small N_2 overpressure.

For the ex situ adsorption process, aqueous solutions with an excess copolymer concentration of 1 mg/mL (PLL(20)-g[2.9]-PEG(2)) and 0.5 mg/mL (PLL(20)-g[3.5]-PEG(5)) were used with an immersion time of 30 min at room temperature (23 °C). Following the adsorption, the samples were thoroughly rinsed with water and mounted into the SFA. Continuously rinsing with ultrapure water during handling was used to prevent unwanted dehydration of the samples.

Measurements of surface−force isotherms were first carried out with one side covered with the polymer film (brush−wall experiment). After that, the adsorption procedure was repeated on the other surface with a fresh polymer solution from the same stock solution to establish an interferometer with both sides covered by a similar polymer layer (brush−brush experiment).

Results and Discussion

Compression Isotherms. The surface-force isotherms measured on the single-sided and double-sided polymer films are shown in Figure 3. The polymer forms a compressible film of about 9 nm thickness and 17 nm thickness for PEG(2) and PEG(5), respectively. The compression of the adsorbed layers leads to a repulsive

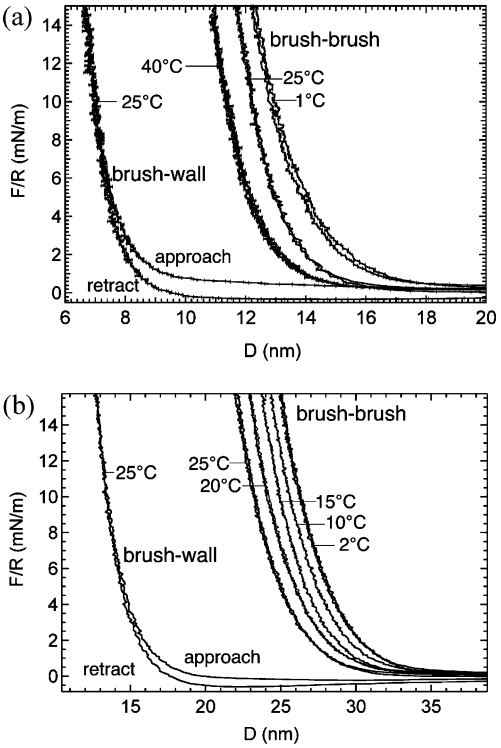

Figure 3. Compression isotherms measured on (a) PLL(20)-g[2.9]-PEG(2) and (b) PLL(20)-g[3.5]-PEG(5) for the brush−wall and brush−brush configuration. In the case of the brush−brush experiment the repulsive force is visible at a greater surface separation than in the brush−wall experiment.

force, which is almost completely elastic. In the case of the brush−wall experiments, there is a weak hysteresis visible in the low-load regime. This small attractive force between the polymer layer and the probing mica surface can be interpreted as the presence of unbound poly-L-lysine segments attracted by the surface charges of the opposing mica surface. At low ionic strengths, no attractive force between the PEG chains and the mica surface is to be expected.[26]

Film Thickness. A measure for the film thickness was obtained by fitting the compression isotherms with Alexander−de Gennes scaling theory[8,27] according to[28]

$$\frac{F(D)}{R} = C_1\left[7\left(\frac{D - mD_0}{mL}\right)^{-5/4} + 5\left(\frac{D - mD_0}{mL}\right)^{7/4} - 12\right] \quad \text{for } D < L \quad (2)$$

with the surface separation D, an offset $D_0 = 1$ nm that accounts for the underlying PLL anchor, the brush length L, $m = 1$ for the brush−wall experiment, and $m = 2$ for the brush−brush experiment. C_1 depends on the grafting density of the PEG chains on the surface. In Figure 4, the same set of data as in Figure 3a after subtraction of the offset (2 nm for the brush−brush and 1 nm for the brush−wall configuration for PLL(20)-g[2.9]-PEG(2)) is shown together with fits from the modified scaling model according to eq 2.

The scaling approach of Alexander and de Gennes[8,27] is based on a steplike density profile of the polymer. This assumption is strictly only valid for very dense brushes, where the chains are nearly completely extended, and the osmotic pressure of the polymer follows a des Cloizeaux behavior.[9] Milner, Witten, and Cates have applied a self-consistent-field theory method for calculating the free energy of the compressed brush,[29,30]

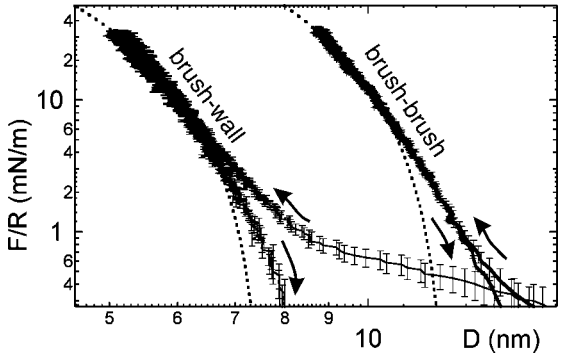

Figure 4. Compression isotherms measured on PLL(20)-g[2.9]-PEG(2) at 25 °C for the brush−wall and the brush−brush experiment. The data sets were shifted by 1 nm (brush−wall) and 2 nm (brush−brush). This offset D_0 accounts for the underlying PLL anchor. The experimental data were fitted with the modified scaling model according to eq 2 (dashed lines, $L = 7.6$ nm for brush−wall and $L = 6.2$ nm for brush−brush).

leading to a parabolic density profile, which is a more realistic description. This theory was developed for infinitely long chains, and though reproducing well the behavior of chains of a polystyrene brush in toluene, containing about a thousand chain segments,[31] it is less appropriate for the analysis of the short chains examined here. However, in the framework of the theory it is possible to describe the effect of polydisperity on the free energy of the brush.[31,32] In the range of small compressions, the slope of the free energy curve is qualitatively altered, growing more slowly with compression.[32]

The temperature dependence of the film thickness for the brush−brush experiment is shown in Figure 5. The film thickness shows a reversible negative temperature dependence. Over the temperature range explored here, the brush lengths scale linearly with a slope of −0.3 Å/K (PEG(2)) and −0.8 Å/K (PEG(5)). This behavior, although not included in the scaling theory, can be explained by the structural solubility of the PEG molecules in water, which causes a decrease in solvent quality with an increase in temperature. Collapse of polymer brushes with decreasing solvent quality is predicted by various theoretical approaches.[33,34]

The negative temperature dependence seen in Figure 5 is related to the large compensation between entropy and enthalpy in hydrated PEG.[35] Various reasons have been put forward for the unusual thermodynamic properties of the PEG−water system. Poly(ethylene glycol) is an amphiphilic molecule that is soluble in water as well as in a variety of organic solvents. This amphiphilic behavior is due to the fact that a conformational change around the C−C bonds of the chains can vary the polarity of the molecule. In a polar solvent, the gauche conformation is more favored because it has a larger dipole moment than the trans conformation.[36,37] In the gauche conformation, the distance between neighboring oxygen atoms in the chain is close to the oxygen−oxygen distance in liquid water,[1] thus enabling the PEG chains to participate in the hydrogen-bonding network of the water by connecting via the two lone pairs of the oxygens of PEG.[38−40] Bridging between oxygen atoms separated by two EG units via a hydrogen-bonded water molecule is possible as well.[41] The increase in the population of the trans conformations at higher temperatures causes a reduced polarity of the PEG chains.[39] In addition, the temperature increase

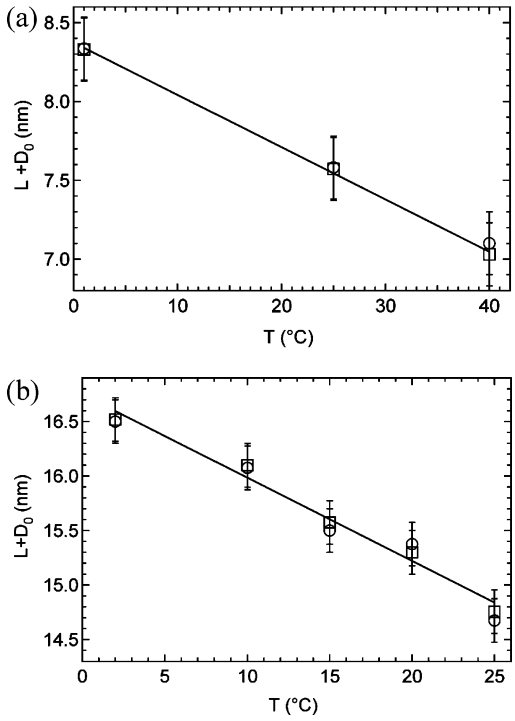

Figure 5. Thickness of the (a) PLL(20)-g[2.9]-PEG(2) and (b) PLL(20)-g[3.5]-PEG(5) films in brush−brush experiments as a function of temperature. Squares: fit with eq 2, offset-corrected; circles: thickness determined by comparing the surface separation at an arbitrary, but small reference load of 0.8 mN/m (a) and 0.6 mN/m (b). Solid line: linear fit of the brush length data set determined with eq 2.

lowers the polymer−water interaction strength and leads to the loss of water molecules that are not tightly bonded to the polymer.[42]

Adsorbed Mass. From the refractive index data, which were collected simultaneously with the compression isotherms, it is possible to extract the amount of polymer adsorbed on the mica surface. The refractive index, $n(D)$ at a distance L between the surfaces, is modeled with[43]

$$n(D) = n_{H_2O} + m\zeta(n_{PEG} - n_{H_2O})/D \quad \text{for } D > \zeta \quad (3)$$

Here, $n = 1.337$ is the refractive index of the aqueous solution, and $n = 1.51$ is the refractive index of the dry PEG polymer. The prefactor is $m = 1$ for the brush−wall experiment, and $m = 2$ for the brush−brush experiment. The equivalent thickness $\zeta = \Gamma/\rho$ of the dried polymer layer is the ratio of the adsorbed PLL-gPEG mass Γ and the dry polymer density $\rho \approx 1.12$ g/cm^3. The experimental data and the result of the fit for PLL(20)-g[2.9]-PEG(2) are shown in Figure 6.

We find that the adsorbed mass of PLL(20)-g[2.9]-PEG(2) and PLL(20)-g[3.5]-PEG(5) films are 200 ± 100 and 160 ± 80 ng/cm^2, respectively. In the case of PLL(20)-g[2.9]-PEG(2), these values are in good agreement with the data for the adsorbed mass of 217 ± 14 ng/cm^2 for PLL(20)-g[3.5]-PEG(2) adsorbed on niobium oxide surfaces determined with optical waveguide lightmode spectroscopy, whereas the value for PLL(20)-g[3.5]-PEG(5) is slightly smaller than the reference value of 247 ± 77 ng/cm^2 on niobium oxide.[11,12] In a previous study, the similarity of the polymer films on mica with the films adsorbed on niobium oxide was shown for PLL(20)-g[3.5]-PEG(2) by means of the quartz crystal microbalance technique.[44]

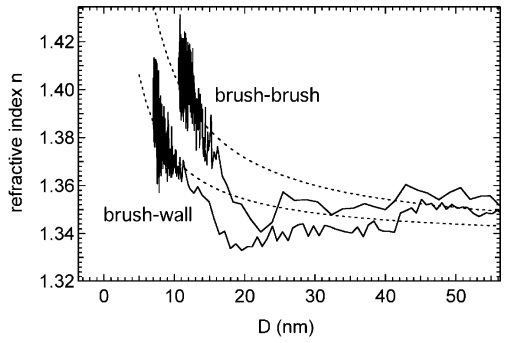

Figure 6. Refractive index data for PLL(20)-g[2.9]-PEG(2). The dashed lines show fits according to eq 3, with an equivalent dry thickness of 2.027 Å, corresponding to an adsorbed mass of 200 ng/cm^2.

On the basis of the adsorbed mass, it is possible to calculate the grafting density of the PEG chains. For PLL(20)-g[2.9]-PEG(2), each PEG chain covers an area of $\Sigma_{PEG(2)} = 7.8$ nm^2 on average. For PLL(20)-g[3.5]-PEG(5) the average areal coverage of a PEG chain is $\Sigma_{PEG(5)} = 22.7$ nm^2.

The Flory radius of the free PEG chains $R_F = aN^{0.6}$ can be calculated with $a = 0.35$ nm, the Kuhn statistical length (which is the effective monomer length),[45] and N, the number of EG units per chain. It is about 3.4 nm for the PEG(2) chains with $N = 45$ and about 6 nm for the PEG(5) chains with $N = 114$ EG units per chain. For a good solvent, such as water, the Flory radius is similar to the radius of gyration of the free polymer chain.[33] If the grafting distance reaches the limit of the radius of gyration, the polymer is extended into a brushlike conformation. For both polymers investigated here, the average distance of the grafting points is significantly smaller than the radius of gyration. At such grafting densities, the polymers are in a brushlike conformation, although both systems are still in the weak overlap regime, where the scaling approach is not strictly valid, since the osmotic pressure in the polymer film is too low.[9] On the other hand, the experimentally measured ratio of the two polymer film thicknesses is in good agreement with the predictions of the scaling theory. In this framework, the film thickness L is proportional to $N^a/\Sigma_{PEG}{}^b$, where N is the number of monomers and Σ_{PEG} is the surface area per PEG chain. For the semidilute brush regime the exponent a is 1 and b is 1/3. This leads to a ratio of the brush lengths $L_{PEG(2)}/L_{PEG(5)} = 0.56$, which is close to the experimental value of 0.53.

Interpenetration of the Brushes. For the analysis of the brush−brush interpenetration, in Figure 7 the data of the brush−wall experiment are plotted against the distance D of the substrate surfaces, whereas the data of the brush−brush experiment are plotted against $D/2$. For both copolymer architectures, the curves of the brush−brush experiments are located at smaller distances than the curves of the brush−wall experiments. This means that the two brushes can overlap for about 2 nm (PEG(2)) and 4 nm (PEG(5)) without raising the repulsive force above the detection limit. In an earlier study, we observed a similar overlap behavior for a slightly different polymer architecture and at a different salt concentration.[28]

The overlap is shown in detail in Figure 8. Here, the overlap ΔD, normalized by L, is plotted vs the separation D normalized by $2L$. L is the brush length of the brush−brush experiment at 25 °C. For both polymers,

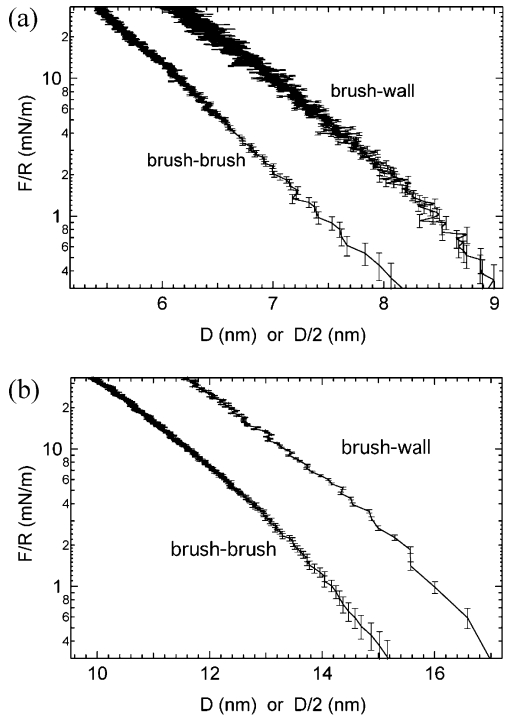

Figure 7. Comparison of the brush−brush and the brush−wall compression for (a) PLL(20)-g[2.9]-PEG(2) and (b) PLL(20)-g[3.5]-PEG(5) at 25 °C. The brush−wall data are plotted against the gap distance D, and the brush−brush data are plotted against $D/2$.

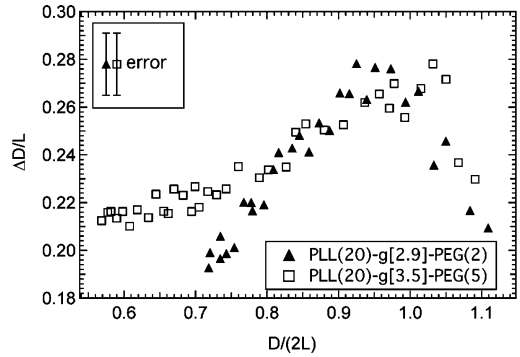

Figure 8. Relative overlap $\Delta D/L$ vs the relative separation of the two surfaces $D/(2L)$ for the retracting curves (reduced number of data points). For normalizing, the brush length L from the brush−brush experiment was used.

the overlap is about 28% of the brush length at the onset of the repulsive force and decreases with increasing compression. It is interesting to note that for PLL(20)-g[2.9]-PEG(2) the maximum is at a separation of about 95% of the brush length, whereas for PLL(20)-g[3.5]-PEG(5) the maximum occurs at a separation of 105%.

The overlap described above can be interpreted as an interpenetration of the two polymer brush layers upon compression. This interpenetration is schematically shown in Figure 9. The repulsive force measured when the two polymer brushes are compressed is a result of the reduction of the conformational space of the polymer chains and therefore a reduction of entropy. When the film is confined by a hard wall, any conformation extended beyond D is excluded. In the case of the brush−brush experiment, at a distance $2D$, the two films start to interpenetrate each other. The number of excluded conformations is, however, much smaller than for a hard wall. There is a significant overlap ΔD while

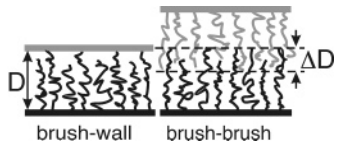

Figure 9. Schematic drawing of the polymer film compressed by a hard wall and a second brush. In the brush−brush experiment, the chains can overlap, whereas in the brush−wall experiment, upon compression any conformation extended beyond the separation is no longer possible.

the repulsive force still remains below the detection limit.

The unperturbed PLL-*g*-PEG films are relatively dilute, containing about 80% water. The adsorption process of the extended poly-L-lysine backbone is random, leading to a nonuniform distribution of the grafting points, and there is a significant contribution of the polydispersity leading to a smooth decrease in the density profile of the polymer film. The large difference between the brush−brush and the brush−wall experiment indicates that the density profile of the polymers has a smooth tail.

In the literature there are only very few reports on experimental comparisons between brush−brush and brush−wall systems. Taunton and co-workers have measured force−distance profiles on polystyrene−PEG block coplymers in toluene and xylene.[46] In these solvents the PEG group adsorbs on the mica surface, whereas the polystyrene chains form a relatively dense brush layer. The brush−wall experiments showed a monotonic repulsive interaction without hysteresis. Although the authors did not expressly quantify their results, a comparison between the brush−wall and the brush−brush experiments shows an overlap of about one-third of the brush length.

Pelletier and co-workers measured the brush−brush and brush−wall force profiles of polystyrene/poly(2-vinylpyridine) in toluene.[47] Here, as well, the polystyrene forms a dense brush, while the poly(2-vinylpyridine) acts as an anchor by adsorbing on the mica surface. However, in contrast to Taunton's work, the brushes showed no overlap but followed the same force curve as the brush−wall setup scaled by a factor of 2.

Interpenetration of polymer brushes has been the subject of studies using a variety of theoretical approaches. It was not included in the scaling theory of Alexander and de Gennes[8,27] or in the self-consistent-field (SCF) approach of Milner, Witten, and Cates,[29,30] which describes the limit of infinite chain length. Martin and Wang used numeric SCF calculations to study the effect of finite chain length.[48] They found that there is a strong effect at the onset of the brush interactions, which is much more pronounced for smaller chains and is very sensitive to interpenetration. Chakrabarti and co-workers,[49] who performed Monte Carlo simulations in a lattice model, showed both interpenetration and compression effects to be present. Whitmore and Noolandi used mean-field SCF theory for the description of the compressed brush.[33] They calculated that the interdigitation of the two opposing polymer brushes is apparent for all surface separations for which the forces are measurable, and each profile of the polymer can reach fully across to the opposite surface. Neelov and co-workers, who used stochastic dynamics simulations to investigate the brush behavior under compression and shear, found that at moderate compressions, where the distance D of the grafting planes is about the length

of the unperturbed polymer film, the interpenetration is restricted to the outermost region.[50]

Conclusions

In aqueous solutions the copolymer PLL-*g*-PEG adsorbes readily onto negatively charged surfaces such as mica. The molecules are anchored via electrostatic interaction of the polylysine backbone with the surface, and the PEG chains form a brushlike film, which is semidilute. The grafting process restricts the density of the PEG brush since the electrostatic attraction of the backbone is balanced by the repulsion of the hydrated PEG chains. Therefore, the grafting density of the film is dependent on the polymer architecture.

Compression isotherms measured in a brush−wall and brush−brush configuration were carried out with the surface forces apparatus. The films show a strong repulsion upon compression. In the brush−wall experiments a small adhesive force was detected.

The thickness of the polymer brush shows a reversible negative temperature dependence, which is a consequence of the structural solubility of PEG in water.

A comparison of compression experiments between the brush−wall and a brush−brush setup shows that a significant overlap of the two brushes is necessary before the repulsive force can be detected. This overlap is interpreted as an interpenetration of the brushes. The shift in the free energy is due to the fact that the restriction of the conformational space of the polymer is much smaller for two opposing brushes than for a brush−wall configuration. It is expected that the interpenetration of the two brushes has an influence on surface properties of the films, such as the frictional behavior.

Acknowledgment. We thank S. Pasche, M. Müller, and F. Durmaz (synthesis of the PLL-*g*-PEG), J. Vörös, A. Rossi, Oleg Borisov, and M. A. Cohen-Stuart (discussions), M. Elsener and J. Vanicek (technical assistance), US Air Force Office of Scientific Research, Contract #F49620-02-1-0346, and TopNano21 Program of the Council of the Swiss Federal Institutes of Technology (ETH-Rat) (financial support).

References and Notes

(1) Kjellander, R.; Florin, E. *J. Chem. Soc., Faraday Trans. 1* **1981**, *77*, 2053−2077.
(2) Napper, D. H. In *Polymeric Stabilization of Colloidal Dispersions*; Ottewill, R. H., Roswell, R. L., Eds.; Academic Press: London, 1983; p 29.
(3) Szleifer, I. *Curr. Opin. Solid State Mater. Sci.* **1997**, *2*, 337−344.
(4) Klein, J.; Kumacheva, E.; Mahalu, D.; Perahia, D.; Fetters, L. J. *Nature (London)* **1994**, *370*, 634−636.
(5) Lee, S.; Müller, M.; Ratoi-Salagean, M.; Vörös, J.; Pasche, S.; De Paul, S. M.; Spikes, H. A.; Textor, M.; Spencer, N. D. *Tribol. Lett.* **2003**, *15*, 231−239.
(6) Müller, M.; Lee, S.; Spikes, H. A.; Spencer, N. D. *Tribol. Lett.* **2003**, *15*, 395−405.
(7) Vermette, P.; Meagher, L. *Colloids Surf. B* **2003**, *28*, 153−198.
(8) de Gennes, P. G. *Adv. Colloid Interface Sci.* **1987**, *27*, 189−209.
(9) Hansen, P. L.; Cohen, J. A.; Podgornik, R.; Parsegian, V. A. *Biophys. J.* **2003**, *84*, 350−355.
(10) Sawhney, A. S.; Hubbell, J. A. *Biomaterials* **1992**, *13*, 863−870.
(11) Kenausis, G. L.; Vörös, J.; Elbert, D. L.; Huang, N. P.; Hofer, R.; Ruiz-Taylor, L.; Textor, M.; Hubbell, J.; Spencer, N. D. *J. Phys. Chem. B* **2000**, *104*, 3298−3309.
(12) Pasche, S.; De Paul, S. M.; Vörös, J.; Spencer, N. D.; Textor, M. *Langmuir* **2003**, *19*, 9216−9225.
(13) Wagner, M. S.; Pasche, S.; Castner, D. G.; Textor, M. *Anal. Chem. A* **2004**, *76*, 1483−1492.
(14) Huang, N. P.; Michel, R.; Vörös, J.; Textor, M.; Hofer, R.; Rossi, A.; Elbert, D. L.; Hubbell, J.; Spencer, N. D. *Langmuir* **2001**, *17*, 489−498.
(15) Pasche, S. Ph.D. Thesis No. 15712, Swiss Federal Institute of Technology (ETH) Zürich, Switzerland, 2004.
(16) Israelachvili, J. N.; McGuiggan, P. M. *J. Mater. Res.* **1990**, *5*, 2223−2231.
(17) Israelachvili, J. N. *J. Colloid Interface Sci.* **1973**, *44*, 259−272.
(18) Heuberger, M. *Rev. Sci. Instrum.* **2001**, *72*, 1700−1707.
(19) Derjaguin, B. *Kolloid Z.* **1934**, *69*, 155−164.
(20) Israelachvili, J. *Intermolecular and Surface Forces;* Academic Press: London, 1992; p 161 ff.
(21) Zäch, M.; Heuberger, M. *Langmuir* **2000**, *16*, 7309−7314.
(22) Heuberger, M.; J. Vanicek, J.; Zäch, M. *Rev. Sci. Instrum.* **2001**, *72*, 3556−3560.
(23) Ohnishi, S.; Hato, M.; Tamada, T.; Christenson, H. K. *Langmuir* **1999**, *15*, 3312−3316.
(24) Kohonen, M. M.; Meldrum, F. C.; Christenson, H. K. *Langmuir* **2003**, *19*, 975−976.
(25) Heuberger, M.; Zäch, M. *Langmuir* **2003**, *19*, 1943−1947.
(26) Chai, L.; Klein, J. *J. Am. Chem. Soc.* **2005**, *127*, 1104−1105.
(27) Alexander, S. *J. Phys. (Paris)* **1977**, *38*, 983−987.
(28) Heuberger, M.; Drobek, T.; Spencer, N. D. *Biophys. J.* **2005**, *88*, 495−504.
(29) Milner, S. T.; Witten, T. A.; Cates, M. E. *Macromolecules* **1988**, *21*, 2610−2619.
(30) Milner, S. T. *Science* **1991**, *251*, 905−914.
(31) Milner, S. T. *Europhys. Lett.* **1988**, *7*, 695−699.
(32) Milner, S. T.; Witten, T. A.; Cates, M. E. *Macromolecules* **1989**, *22*, 853−861.
(33) Whitmore, M. D.; Noolandi, J. *Macromolecules* **1990**, *23*, 3321−3339.
(34) Zhulina, E. B.; Borisov, O. V.; Priamitsyn, V. A. *J. Colloid Interface Sci.* **1990**, *137*, 495−511.
(35) Kingman, N. G.; Rosenberg, A.; Bastos, M.; Wadsö, I. *Thermochim. Acta* **1990**, *169*, 339−346.
(36) Karlström, G. *J. Phys. Chem.* **1985**, *89*, 4962−4964.
(37) Begum, R.; Matsuura, H. *J. Chem. Soc., Faraday Trans.* **1997**, *93*, 3839−3848.
(38) Jannelli, M. P.; Magazu, S.; Maisano, G.; Majolino, D.; Migliardo, P. *J. Mol. Struct.* **1994**, *322*, 337−343.
(39) Björling, M.; Karlström, G.; Linse, P. *J. Phys. Chem.* **1991**, *95*, 6706−6709.
(40) Matsuura, H.; Fukuhara, K. *J. Mol. Struct.* **1985**, *126*, 251−260.
(41) Tasaki, K. *J. Am. Chem. Soc.* **1996**, *118*, 8459−8469.
(42) Branca, C.; Magazu, S.; Maisano, F.; Migliardo, F.; Migliardo, P.; Romeo, G. *J. Phys. Chem. B* **2002**, *106*, 10272−10276.
(43) Raviv, U.; Frey, J.; Sak, R.; Laurat, P.; Tadmor, R.; Klein, J. *Langmuir* **2002**, *18*, 7482−7495.
(44) Heuberger, M.; Drobek, T.; Vörös, J. *Langmuir* **2004**, *20*, 9445−9448.
(45) Kenworthy, A. K.; Hristova, K.; Needham, D.; McIntosh, T. J. *Biophys. J.* **1995**, *68*, 1921−1936.
(46) Taunton, H. J.; Toprakcioglu, C.; Fetters, L. J.; Klein, J. *Macromolecules* **1990**, *23*, 571−580.
(47) Pelletier, E.; Belder, G. F.; Hadziioannou, G.; Subbotin, A. *J. Phys. II* **1997**, *7*, 271−283.
(48) Martin, J. I.; Wang, Z.-G. *J. Phys. Chem.* **1995**, *99*, 2833−2844.
(49) Chakrabarti, A.; Nelson, P.; Toral, R. *J. Chem. Phys.* **1994**, *100*, 748−749.
(50) Neelov, I. M.; Borisov, O. V.; Binder, K. *J. Chem. Phys.* **1998**, *108*, 6973−6988.

MA0504217